XII International Conference on Textile Composites and Inflatable Structures
STRUCTURAL MEMBRANES 2025
R. Wüchner, A. K. Goldbach, R. Rossi and C. Lázaro (Eds)

THE EFFECT OF SLITS AND NOTCHES IN FABRIC SPECIMENS UNDER BIAXIAL TENSION

M. Boljen*, F. Kölble*, W. Harwick*, and R. Taylor†

* Fraunhofer Institute for High-Speed Dynamics, Ernst-Mach-Institut, EMI,
Ernst-Zermelo-Str. 4, 79104 Freiburg, Germany,
e-mail: matthias.boljen@emi.fraunhofer.de, web page: https://www.emi.fraunhofer.de/

† Ove Arup & Partners International Ltd.,
8F Iidabashi Grand Bloom, 2-10-2 Fujimi Chiyoda-ku, Tokyo 102-0071, Japan,
web page: https://www.arup.com/

Key words: Airbag fabrics, mechanical characterization, biaxial tensile tests, shape optimization

Summary. Different specimen types and test setups have been developed over time for biaxial tensile testing of woven fabrics. Due to the technical requirement to fix specimens at the clamps of the tensile tester and the associated kinematic constraint on the lateral movement, biaxial stress usually cannot be distributed purely homogenously throughout the specimen. In this study, different specimen types are analyzed numerically with respect to the best stress distribution possible. The occurence of stress concentrations and potential restrictions upon the specimen's ultimate failure limit resulting from unfavourable geometries are identified. An idealized quadratic specimen's geometry with free lateral movement is selected as academic reference. Special focus is put on the transition from quadratic to cruciform shapes and the effects arising from the integration of slits and notches. Experimental results for selected geometries are compared to numerical simulations and discussed with respect to recommendations found in literature. Cruciform specimens with integrated slits perform best with regard to the generation of pure biaxial tension, whereas quadratic specimens suffer from premature failure before reaching the ultimate failure strain of the fiber material. The integration of curved notches inbetween the specimen's legs slightly improves the performance of quadratic specimens only.

1 INTRODUCTION

With the automotive industry moving into the era of virtual testing which requires "out-of-the-box" predictions from highly complex airbag simulations, there is a rapidly increasing demand for more accurate fabric characterization methods. Numerical simulations have to be predictive over a wide range of applications without intermediate component testing, which requires reliably calibrated fabric material models in the first place. For the numerical assessment of airbags, explicit finite element solvers usually invoke constitutive models that capture the fabric behaviour by two unidirectional layers of fibers exhibiting nonlinear stress-strain behaviour along warp and weft directions. The material response due to fiber straining is often defined using tabular stress-strain

data relating longitudinal stress with longitudinal strain. This relationship can be extended to include also strain rate, temperature or transversal strain. To calibrate these models, the mechanical behaviour of the fabric material needs to be characterized using inplane shear tests and biaxial tensile tests. For the latter and the conversion of loadcell forces $F_i(t)$ into second Piola-Kirchhoff stresses to be accurate, a uniform stress distribution in warp and weft direction is needed and has to be as close to a pure biaxial stress condition as possible. Second Piola-Kirchhoff stresses S_i and Green-Lagrange strains E_i can easily be obtained from engineering stresses σ_i and engineering strains ε_i using the following conversion formulae:

$$E_i = \frac{1}{2}\left[\left(1+\varepsilon_i\right)^2 - 1\right] \qquad \text{where} \qquad \varepsilon_i = \frac{d_i}{L}, \tag{1}$$

$$S_i = \frac{\sigma_i}{1+\varepsilon_i} \qquad \text{where} \qquad \sigma_i = \frac{F_i}{wH}. \tag{2}$$

In the above equations, the specimen's displacement over time is denoted using $d_i(t)$. The specimen's dimensions in the initial undeformed state are described using its free length L, its section width w and its thickness H. Whereas shear testing using picture-frame devices allows to subject the specimen homogenously to a state of pure shear, subjecting a specimen to pure biaxial tension is physically difficult to achieve since the applied pressure of the clamps restricts lateral motion of the specimen. Different specimen types and testing devices have evolved over time to resolve this as demonstrated by Bridgens [1], Ballhause [2], Colasante [3] and van Craenenbroeck [4].

2 METHODS

2.1 Test environment

The multiaxial tensile testing facility used in this study is shown in Figure 1. Four clamps are arranged inplane and at orthogonal angles. The clamps are displacement-driven and equipped with piezoelectric sensors able to measure forces up to 15 kN. A clamping profile of 80 mm width transitioning from sinusoidal to trapezoidal shape is used to grip the fabric samples. Strain rates may vary from quasi-static up to $1\,\mathrm{s}^{-1}$. For elevated temperatures, the facility can be equipped with an optional chamber allowing temperatures between $-40\,^{\circ}\mathrm{C}$ and $120\,^{\circ}\mathrm{C}$ as shown in previous studies [5]. Videos of deforming specimens are recorded in this study using a Basler acA2040 GigE camera with a resolution of $1280\,\mathrm{px} \times 1280\,\mathrm{px}$ and a frame rate of 5 Hz. Digital image correlation for tracking local deformations on the specimen is implemented using GOM Professional 2017 for point tracking in 1D and 2D. The material has been tested under an ambient temperature of $23\,^{\circ}\mathrm{C}$, at 50 % relative humidity and approximatively 101 kPa ambient pressure.

2.2 Simulation environment

In this study, the material model `*MAT_FABRIC` of the explicit finite element solver LS-DYNA [6] is applied. The model is calibrated for large strains with orthogonal material angles and nonlinear stress strain behavior (`FORM = 14`). Only uniaxial load curves (`LCA`, `LCB`) and unload curves (`LCUA`, `LCUB`) are taken into account. Reloading has been calibrated to follow an intermediate slope between

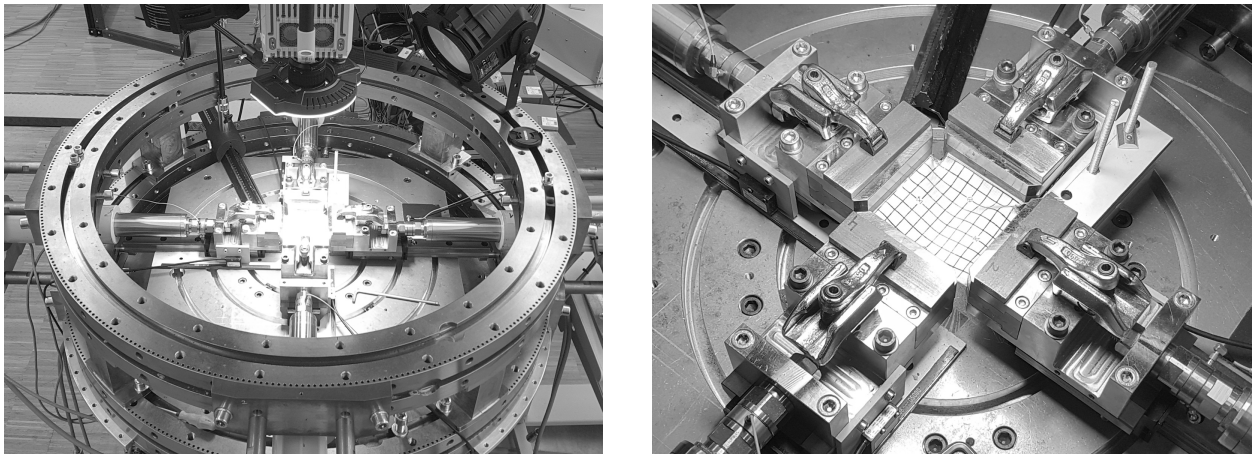

(a) Test facility

(b) Test setup

Figure 1: Testing environment: (a) test facility, (b) test setup.

unloading and loading curve (`RL = 0.5`). Compressive fiber stresses are eliminated (`CSE = 1`). For the silicone rubber coating, an elastic liner (`EL = 10 MPa`, `PRL = 0.49`) with a small volume fraction (`LRATIO = 0.01`) is added to stabilize the material under compression. Rayleigh damping is slightly increased (`DAMP = 0.1`). All other model parameters remain as default. The selected material model is invoked at each integration point for all elements of the spatial discretization of the fabric specimens. In this study, fully integrated Belytschko-Tsay membranes are applied (`ELFORM = 9`) using one through-thickness integration point (`NIP = 1`). The material angles of warp and weft yarn direction are defined orthogonally (`B1 = 0`, `B2 = 90`), whereas warp direction (A) is modelled collinear with the global Y direction, and weft direction (B) is collinear with the global X direction. All models were run using the explicit FE solver LS-DYNA release 16.1, in single precision. The platform in use was a Xeon64 System using CentOS Linux release 7.9. All runs have been processed using 12 cores and without any mass scaling to not artificially increase the minimum allowed time-step.

2.3 Specimens

The material used in this study is a silicone rubber coated, woven fabric material made from polyamide PA 6.6 fibers. Basic material properties with respect to the fabric weave, thickness, areal weight and physical density are given in Figure 2. Ten specimen types were selected for numerical analysis. Figure 3 shows the specimens selected for experimental testing, i.e. the quadratic notched (QN), the cruciform (C), and the slit cruciform (CS) shape. An academic specimen (A) with free lateral clamp movement and two miniaturized specimen shapes with (MS) and without slits (M) are shown in Figure 4. The former was used as a theoretical best reference for comparison to other specimen types, the latter to gain insight into the feasibility of reducing specimen size to reach higher strain rates with the same tensile tester in future work. All specimen types including basic dimensions and FE model data are shown in Table 1.

(a) Image

Property	Unit	Value
Weave pattern	-	Plain
Fiber material	-	PA 6.6
Coating material	-	Silicone
Linear density	dtex	470
Yarn strength	N	40
Failure strain	%	20
Yarn count	cm^{-1}	18
Areal weight	$\mathrm{g\,m}^{-2}$	203
Thickness	mm	0.249
Density	$\mathrm{g\,cm}^{-3}$	0.818

(b) Basic properties

Figure 2: Test material: (a) image, (b) basic properties.

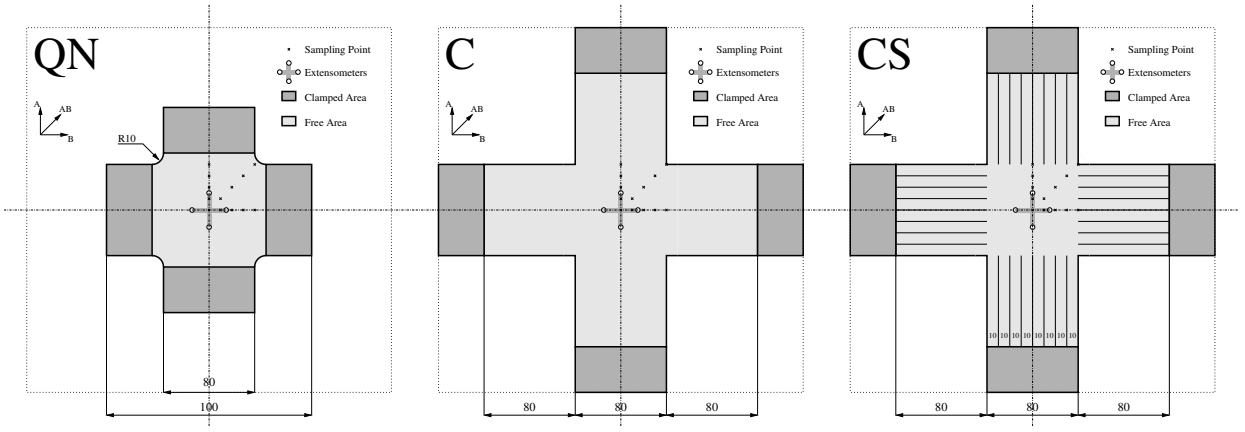

(a) Type QN **(b)** Type C **(c)** Type CS

Figure 3: Specimen types selected for testing: (a) quadratic shape, (b)–(c) cruciform shapes.

2.4 Test matrix

All specimens are loaded biaxially to a nominal tensile strain of 15 % using a constant velocity and a strain rate of approximatively $0.0075\,\mathrm{s}^{-1}$. Due to the different specimen dimensions, the individual clamp velocities vary between $375\,\mu\mathrm{m\,s}^{-1}$ for the quadratic and miniaturized specimens and $900\,\mu\mathrm{m\,s}^{-1}$ for the cruciform specimens. After loading, the specimens will be fully unloaded and reloaded until failure using the same velocity. Figure 5 verifies that the nominal clamp displacement used for the model deformation is correctly reproduced. Clamp displacement along warp and weft directions is normalized with respect to the initial distance for better comparison. The nominal curves used for the simulation models were slightly modified from the experimental curve to account for slippage observed at tensile strains higher than 15 % ($t > 60\,\mathrm{s}$). Experiments have been repeated using 3 different samples for each specimen type to check reproducability.

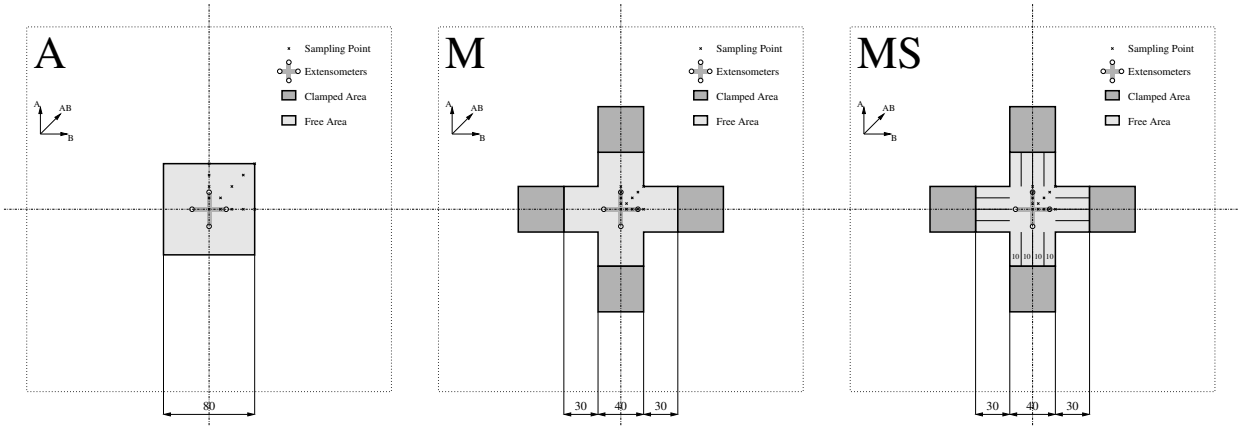

(a) Type A **(b)** Type M **(c)** Type MS

Figure 4: Additional specimen types: (a) academic shape, (b)–(c) miniaturized shapes.

Table 1: Analyzed specimen geometries, basic dimensions and finite element model data.

Type	**Shape**	**Slit**	**Notch**	**Tests**	**Length** mm	**Width** mm	**Area** cm^2	**Nodes**	**Elements**
A	academic	no	no	no	80	80	64	1200	1020
Q	quadratic	no	no	no	100	80	96	1900	1540
QN		no	yes	yes					
C	cruciform	no	no	yes	240	80	320	6300	5120
CN		no	yes	no					
CS		yes	no	yes					
CSN		yes	yes	no					
M	miniaturized	no	no	no	100	40	64	1300	1020
MN		no	yes	no					
MS		yes	no	no					
MSN		yes	yes	no					

3 RESULTS

3.1 Test data

Images of the biaxial tensile tests for the specimen types QN and CS at various points in time along the applied sequence of loading, unloading and reloading are shown in Figure 6 and Figure 7, respectively. Failure takes place as expected at strains around $18 \pm 2\,\%$ which is close to the ultimate fiber strain of the test material. Crack initiates at failing weft yarns in the area between the specimen's legs. Figure 8 shows the averaged stress-strain data extracted from experiments for each specimen type. Obviously, the quadratic specimens show a stiffer response and seem to fail prematurely compared to the crucifrom specimens indicating a drawback of the quadratic type.

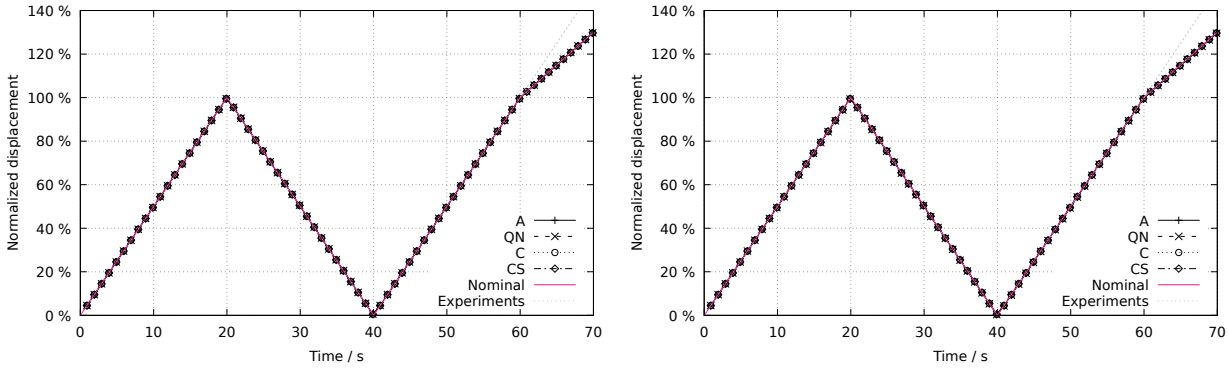

(a) Warp direction **(b)** Weft direction

Figure 5: Normalized clamp displacement with respect to undeformed specimen length for selected specimen types in (a) warp and (b) weft direction. Nominal displacement is used for simulation models to include specimen slippage observed in experiments ($t > 60\,\mathrm{s}$).

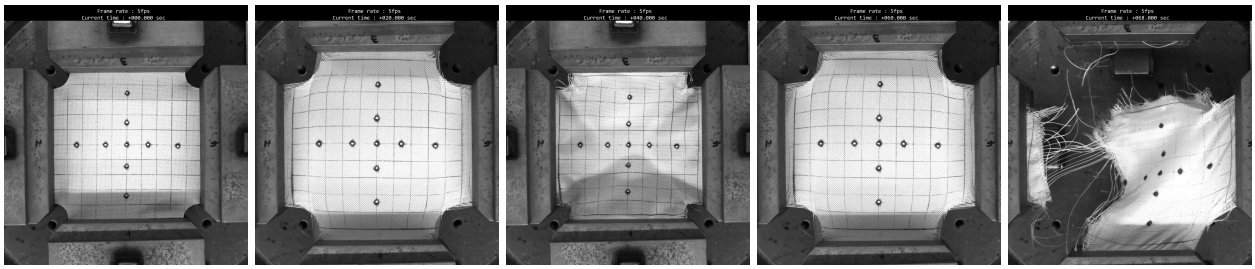

(a) 0 s **(b)** 20 s **(c)** 40 s **(d)** 60 s **(e)** 68 s

Figure 6: Still images of biaxial testing of the quadratic notched specimen type QN at various stages of the loading sequence: (a) undeformed, (b) loaded, (c) unloaded, (d) reloaded, (e) failed.

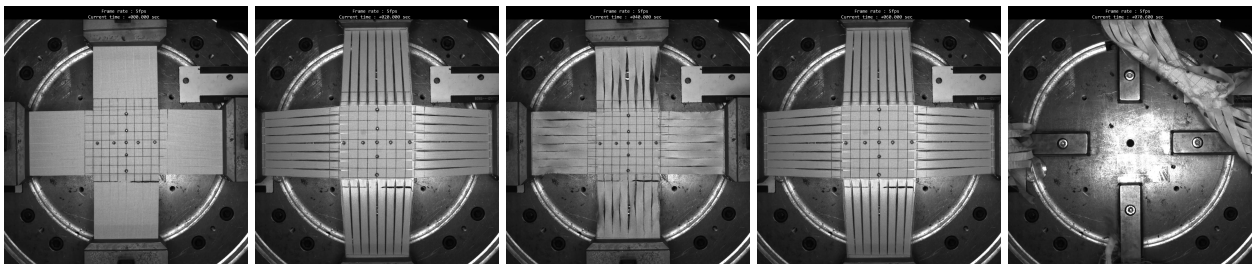

(a) 0 s **(b)** 20 s **(c)** 40 s **(d)** 60 s **(e)** 71 s

Figure 7: Still images of biaxial testing of the slit cruciform specimen type CS at various stages of the loading sequence: (a) undeformed, (b) loaded, (c) unloaded, (d) reloaded, (e) failed.

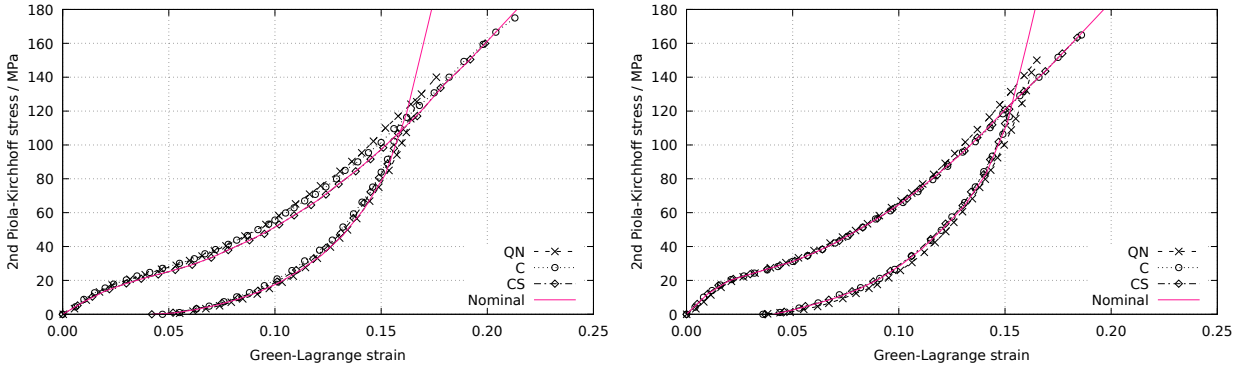

(a) Warp direction **(b)** Weft direction

Figure 8: Experimentally derived stress-strain data for selected specimen types in (a) warp and (b) weft direction. Specimen type QN shows a stiffer response and fails to an earlier point in time compared to types C and CS.

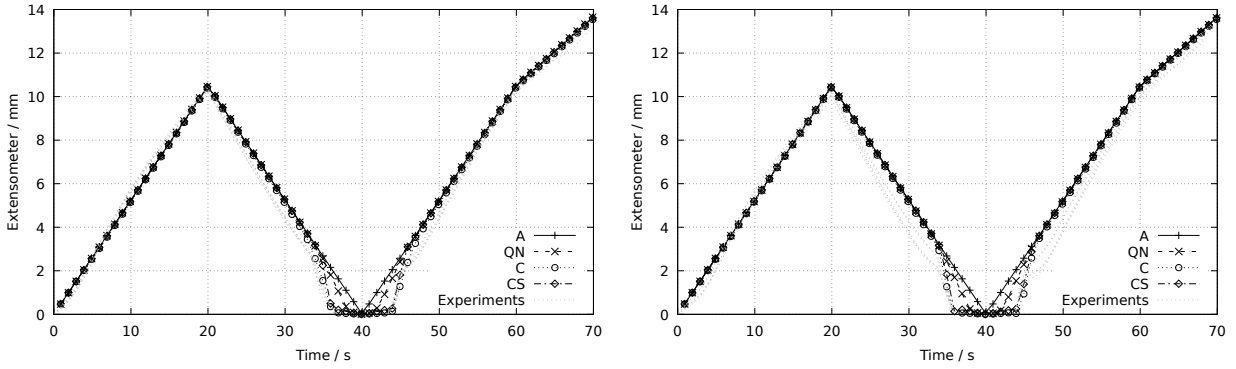

(a) Warp direction **(b)** Weft direction

Figure 9: Extensometer elongations for selected specimen types in (a) warp and (b) weft direction.

3.2 Model prediction

For the simulation models, only the stress-strain data taken from the cruciform slit (CS) tests has been applied. Figure 9 shows a comparison of the experimentally and numerically determined extensometer elongations at the specimen's center. Deviations with respect to the clamp displacement usually occur due to necking or clamp slippage. Since unloading of the specimen's center is completed more quickly compared to the specimen's legs, some wrinkling and out-of-plane movement of the material can be observed in the experiments as well as in the simulations ($35\,\mathrm{s} < t < 45\,\mathrm{s}$). The larger the area of the specimen's legs compared to the center area, the higher is the deviation of the extensometer from the nominal clamp displacement. Figure 10 shows the measured and predicted force histories along warp and weft direction. Though the width w and the thickness H of the cross sections as well as the tensile strains ε_i captured by the extensometers are identical for all specimen types, the predicted force signal F of the quadratic specimen deviates significantly from the cruciform specimens, which makes direct validation of stress-strain data with test data

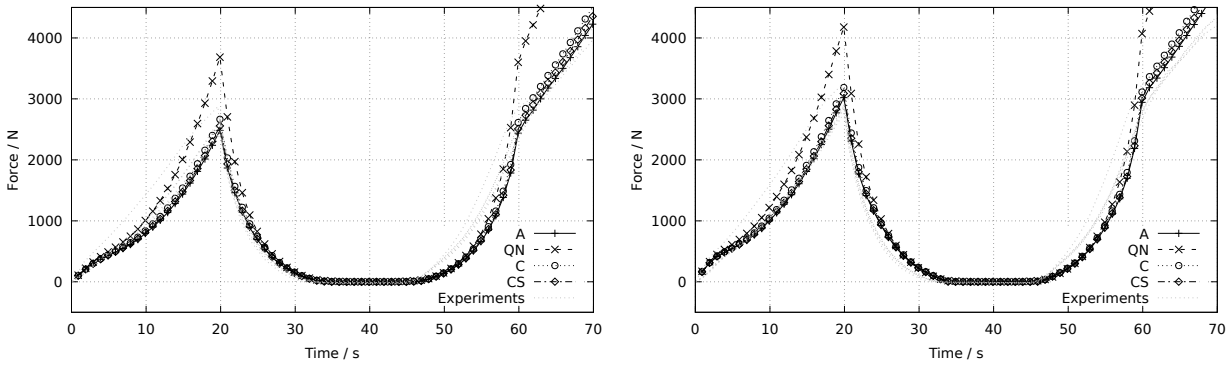

(a) Warp direction **(b)** Weft direction

Figure 10: Force signals at clamps for selected specimen types in (a) warp and (b) weft direction.

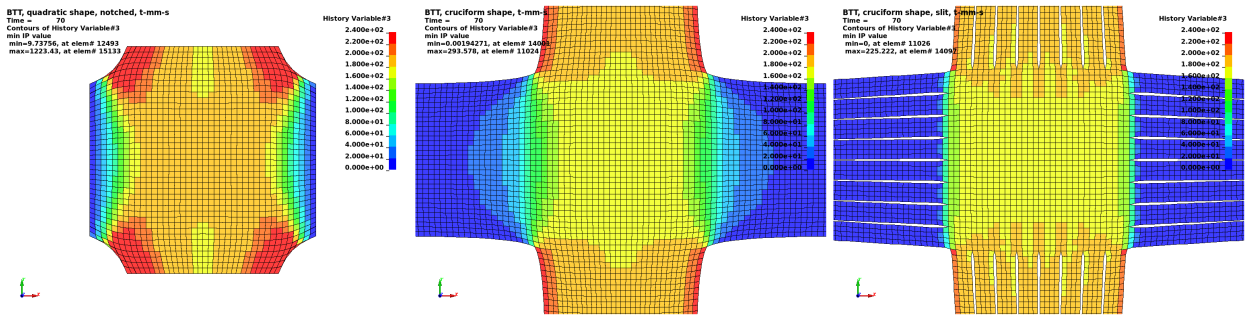

(a) Type QN **(b)** Type C **(c)** Type CS

Figure 11: Stress distribution in warp direction for selected specimen types.

impossible. Moreover, since the lateral movement is restricted for the quadratic specimens, stress concentrations near the corners of the free surface seem to initiate failure before the ultimate fiber failure strain is reached leading to potentially insufficient stress-strain data sets.

3.3 Distributions

For the inspection of the stress tensor components, colored contour plots of the spatial stress distribution are presented for experimentally tested specimen types QN, C and CS. Obviously, the predicted fiber stresses for the quadratic notched specimen near the corners exceed the theoretical failure limit of approximatively 289 MPa (Figure 11 and Figure 12). Since no damage is not considered in the model, failure is not captured numerically. Nevertheless, the crack initiation observed in the experiments is confirmed by the predicted stress level in the models. The distribution of fiber stresses is more uniform for the cruciform specimen type without slits, altough stress intensities are still high especially near the edges of the specimen's legs. The best result with respect to stress intensity and homogeniousity is obtained using the slit cruciform specimen. The integration of slits to the legs of the cruciform specimen type also effectively mitigates spurious domains of resistance to shear deformation (Figure 13). The above findings are confirmed with

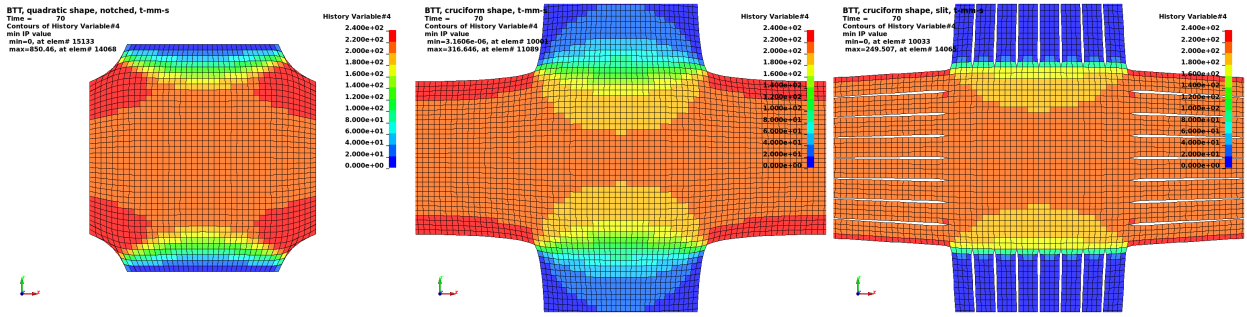

(a) Type QN **(b)** Type C **(c)** Type CS

Figure 12: Stress distribution in weft direction for selected specimens.

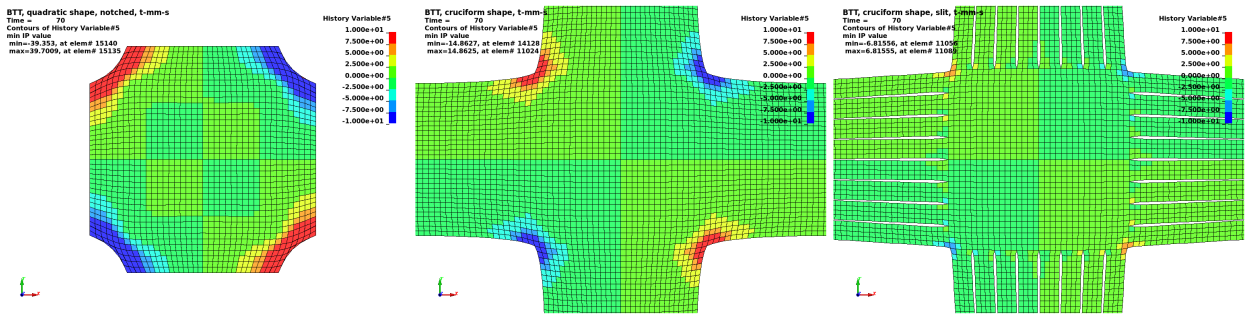

(a) Type QN **(b)** Type C **(c)** Type CS

Figure 13: Shear stress distribution for selected specimen types.

respect to the distribution of the triaxiality factor TF that is universially defined as the ratio of the hydrostatic stress σ_h to the von Mises equivalent stress σ_v:

$$\mathrm{TF} = \frac{\sigma_h}{\sigma_v} = \frac{\frac{1}{3}\left(\sigma_x + \sigma_y + \sigma_z\right)}{\sqrt{\frac{1}{2}\left[\left(\sigma_x - \sigma_y\right)^2 + \left(\sigma_y - \sigma_z\right)^2 + \left(\sigma_z - \sigma_x\right)^2 + 6\left(\tau_{xy}^2 + \tau_{yz}^2 + \tau_{xz}^2\right)\right]}}. \tag{3}$$

The stress distribution in the specimen's center is closest to a pure biaxial state for the cruciform slit type where stress triaxiality is close to TF = 0.667, whereas the stress state in the specimen's legs is close to uniaxial, i.e. TF = 0.333 (Figure 14).

3.4 Sampling points

Sampling points have been selected at various locations with varying distance to the specimen's center in order to gather data for quantitative comparison of the specimen types. At each sampling point, the development of the stress tensor components and the triaxiality factor (3) is monitored. Besides one sampling point at the specimen's center, four equidistant points along three distinct directions are selected, i.e. the warp yarn direction, $\mathrm{A}_i \; \forall \; i \in \{1,2,3,4\}$, the weft yarn direction, $\mathrm{B}_i \; \forall \; i \in \{1,2,3,4\}$, and the diagonal direction, $\mathrm{AB}_i \; \forall \; i \in \{1,2,3,4\}$. Higher indices indicate

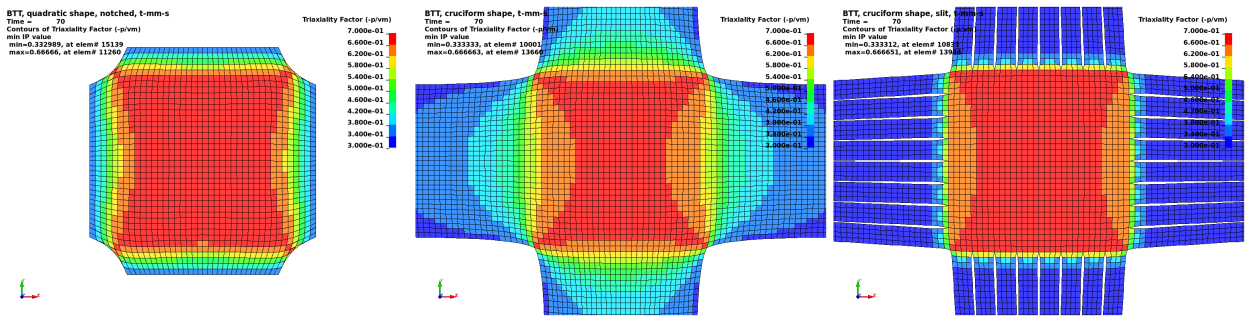

(a) Type QN **(b)** Type C **(c)** Type CS

Figure 14: Stress triaxiality distribution for selected specimen types.

sampling points located closer to the boundary of the biaxially loaded domain of the specimen. Figure 15 shows all identified stress tensor components and the corresponding triaxiality factors at the end of the initial loading phase ($t = 20\,\mathrm{s}$). Since the results for the sampling points with the lower indices do no differ significantly from those of the center point, only the results of the outer sampling points 3 and 4 have been included in the histograms.

3.5 Load score

Each specimen type is compared against the best stress state distribution possible, i.e. the results of the academic specimen type A. In order to have a scalar rating, a certain metric X has to be defined as quantitative measure. An equivalent load score X_i at a certain sampling point i is therefore defined as follows:

$$X_i = \frac{\langle \sigma_{A,i} \rangle + \langle \sigma_{B,i} \rangle}{2\, R_\mathrm{m}} \cdot \frac{\mathrm{TF}_i}{2/3}, \tag{4}$$

whereas the constant parameter R_m may denote either the overall material strength or an arbitrary reference stress level. In this study, a value of $R_\mathrm{m} = 121\,\mathrm{MPa}$ has been selected to match the corresponding stress state of specimen type at the end of the initial loading phase ($t = 20\,\mathrm{s}$). Finally, the root mean square deviation (RMSD) of this load score parameter X_i of all sampling points i of any specimen type compared to the reference sample type A is calculated. If $X_1, ..., X_n$ is a certain population of sampling points i (observation) with true mean value x_0 (prediction), then the RMSD of the chosen population is:

$$\mathrm{RMSD} = \sqrt{\frac{1}{n} \sum_{i=1}^{n} \left(X_i - x_0\right)^2}. \tag{5}$$

Lower RMSD values indicate a better performance with respect to stress intensity and stress homogeniousity compared to the prediction of the academic specimen type. Figure 16 contains the load scores for all specimens analyzed in this study including those experimentally tested as well as all RMSD values and their corresponding standard deviations. As an overall result, the slit cruciform type CS scored the best results compared to the performance of the academic reference type (RMSD) and internal scatter of the sampling point selection (standard deviation).

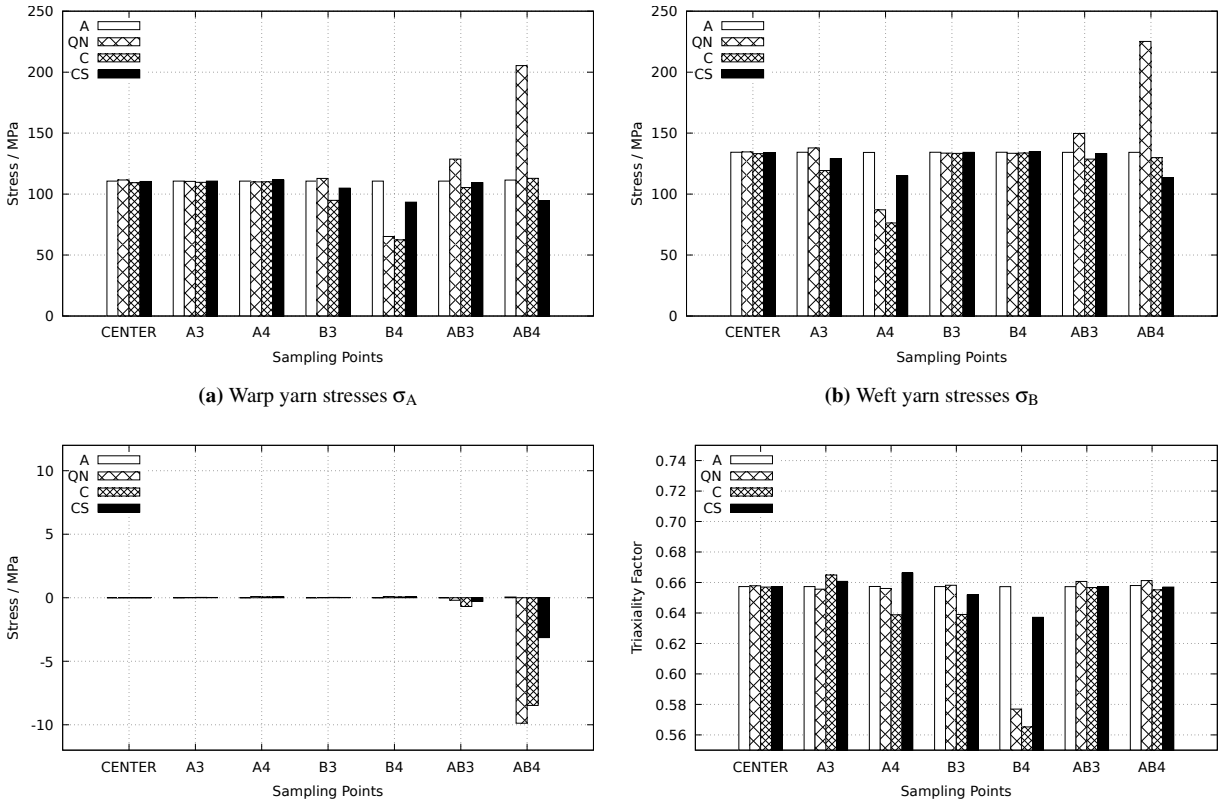

(a) Warp yarn stresses σ_A

(b) Weft yarn stresses σ_B

(c) Shear stresses τ_{AB}

(d) Triaxiality Factor

Figure 15: Local stresses and triaxialities at various sampling points for selected specimen types at the end of the initial loading phase ($t = 20\,\mathrm{s}$).

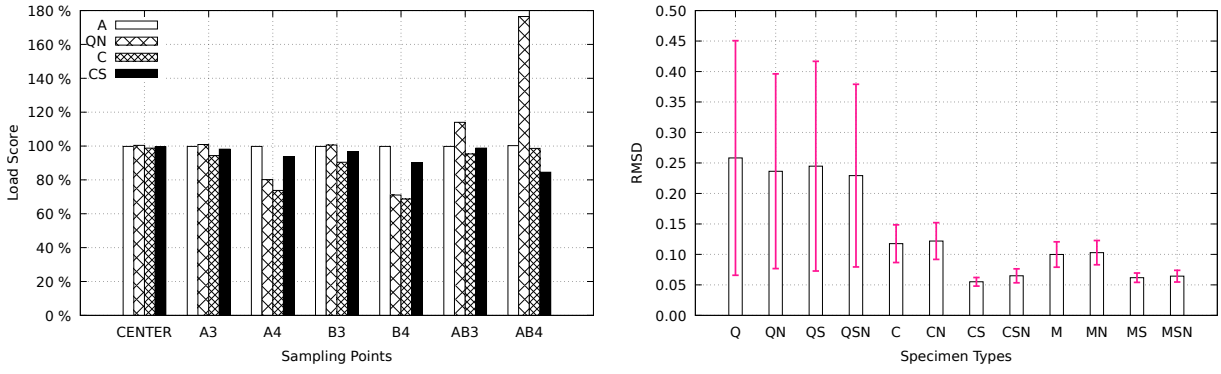

(a) Load score

(b) RMSD

Figure 16: Load indices at various sampling points at the end of the initial loading phase ($t = 20\,\mathrm{s}$): (a) relative values for selected specimens with respect to load level of academic type, (b) RMSD including standard deviation for all specimen types of interest.

4 DISCUSSION

Fabric specimen types for biaxial tensile testing have been compared to an academic specimen type that allows lateral movement at the clamps and is capable of developing a pure biaxial state of tensile stress. A load score has been introduced to relate stresses observed in experiments and simulations, and to obtain a scalar metric for rating. For comparison, the RMSD of each specimen type has been calculated with respect to the prediction given by the academic specimen type. A RMSD of 24 ± 16 % for the quadratic notched type QN compared to the academic type can be reduced to a value of 12 ± 3 % when switching to the cruciform shaped type C. With the introduction of slits to the specimen's legs, the performance can be improved even more with a RMSD of 6 ± 1 % for the slit cruciform type CS which finally marks the best result of all analyzed samples (Figure 16b). Though not experimentally validated, the quadratic notched specimen is probably superior to the quadratic type Q without notches where a RMSD of 26 ± 19 % has been determined. For the cruciform shapes, the addition of curved notches would slightly reduce performance.

5 CONCLUSIONS

Cruciform specimens with integrated slits are recommended for biaxial tensile testing since they provide the closest match to pure biaxial stress conditions throughout the biaxially loaded domain of the specimen. Quadratic specimens tend to develop stress peaks near the notches between the specimen's legs, potentially leading to premature failure and insufficient data sets. Moreover, the force signal relating longitudinal stress to longitudinal strain is over-estimated due to the erroreous influence of the lateral clamps nearby. Miniaturized cruciform specimens promise to be a good alternative to larger cruciform samples with comparable performance.

For accurate mechanical characterization, precise force and displacement measurements and perfect biaxial stress conditions are required. As long as the lateral movement of the specimens at the clamps is constrained, long specimen legs are needed to facilitate lateral movement of the biaxially deformed material domain in the center of the specimen. Self-arresting systems using welded or sewed loops around smooth wedges should be investigated to circumvent slippage observed in the experiments of this study.

Specimen shape optimization should be investigated further in more detail using design of experiment campaigns to tune specimen dimensions and parameters and more testing in order to obtain more robust data for validation. Furthermore, practical criteria need to be taken into consideration, e.g. specifications regarding specimen fabrication, potential exposure to pre-damage during handling and alignment requirements during test preparation.

REFERENCES

[1] Bridgens (2005). *Architectural fabric properties: Determination, representation & prediction*, PhD thesis, Newcastle University.

[2] Ballhause (2007). *Diskrete Modellierung des Verformungs- und Versagensverhaltens von Gewebemembranen*, PhD thesis, Universität Stuttgart.

[3] Colasante (2014). *Tensile structures: Biaxial testing and constitutive modelling of coated fabrics at finite strains*, PhD thesis, Politecnico di Milano.

[4] Van Craenenbroeck (2016). *Biaxial testing of fabrics – Test methodologies and their impact on material parameters and the structural design process*, PhD thesis, Vrije Universiteit Brussel.

[5] Boljen, Rack, Kölble, Rodinger, Harwick (2018). *Characterization and modeling of airbag fabrics subjected to asymmetric biaxial loading and elevated temperatures*, Airbag Symposium, Mannheim.

[6] LS-DYNA Keyword User's Manual, Volume 2, Material Models, R16, ANSYS (2025)